

THE CATALOGUE OF POSITIONS OF OPTICALLY BRIGHT EXTRAGALACTIC RADIO SOURCES OBRs-2

L. PETROV

Astrogeo Center, Falls Church, VA 22043, USA
(Received 2013, January 23; Accepted; Published)

ABSTRACT

It is anticipated that future space-born missions, such as *Gaia*, will be able to determine in optical domain positions of more than 100, 000 bright quasars with sub-mas accuracies that are comparable to very long baseline interferometry (VLBI) accuracies. Comparisons of coordinate systems from space-born missions and from VLBI will be very important, first for investigation of possible systematic errors, second for investigation of possible shift between centroids of radio and optical emissions in active galaxy nuclei. In order to make such a comparison more robust, a program of densification of the grid of radio sources detectable with both VLBI and *Gaia* was launched in 2006. In the second observing campaign a set of 290 objects from the list of 398 compact extragalactic radio sources with declinations $> -10^\circ$ was observed with the VLBA+EVN in 2010–2011 with the primary goal of producing their images with milliarcsecond resolution. These sources are brighter than 18 magnitude at V band. In this paper coordinates of observed sources have been derived with milliarcsecond accuracies from analysis of these VLBI observations following the method of absolute astrometry and their images were produced. The catalogue of positions of 295 target sources and estimates of their correlated flux densities at 2.2 and 8.4 GHz is presented. The accuracies of source coordinates are in a range of 2 to 200 mas, with the median 3.2 mas.

Subject headings: astrometry — catalogues — surveys

1. INTRODUCTION

The method of Very Long Baseline Interferometry (VLBI) first proposed by Matveenko et al. (1965) allows us to derive source positions with nanoradian precision (1 nrad \approx 0.2 mas). Since 1971 when the first catalogue of source coordinates determined with VLBI was published (Cohen & Shaffer 1971), the number of extragalactic compact radio sources which positions were derived using VLBI under absolute astrometry observing programs grew from 35 objects to 7215 in 2012¹. For 95% these sources, accuracies of their positions are in a range of 0.05 to 6.5 mas with the median 0.5 mas. These sources form a dense grid on the sky that can be used for many applications, such as differential astrometry, phase-referencing VLBI observations of weak objects, space navigation, Earth orientation parameter determination, and space geodesy.

However, high accuracy of positions of these objects can be exploited *directly* only by applications that utilize the VLBI technique. Applications that use different observational techniques can benefit from the high accuracy of VLBI positions only *indirectly* by observing common objects from the VLBI catalogue with instruments at other wavelengths. The European Space Agency space-born astrometry mission *Gaia*, scheduled to be launched in 2013, according to Lindegren et al. (2008) promises to reach sub-mas accuracies of determining positions of quasars of 16–20 magnitude that will rival accuracies of absolute astrometry VLBI. Since position catalogues produced with *Gaia* and VLBI will be completely independent, their mutual rotations, zonal differences and possibly other systematic effects can be interpreted as errors of one of the techniques after resolving the differences due to a misalignment of centers of optic and radio images of quasars and a frequency-dependent core-shift (Kovalev et al. 2008; Porcas 2009; Sokolovsky et al. 2011). Investigation of

systematic differences will be very important for the assessment of the overall quality of *Gaia* results and, possibly, the errors in the VLBI position catalogue.

This comparison will produce valuable results if 1) it will be limited to those common sources which VLBI positions are known with errors smaller than several tenths of a milliarcsecond; 2) the number of sources will be large enough to derive meaningful statistics; and 3) the sources will be uniformly distributed over the sky. However, the number of quasars that have a compact core and are bright in both optical and radio wavelengths, and therefore, can be detected with both techniques, currently is rather limited. The observing program for densification of the list of such objects was launched in 2006 (Bourda et al. 2008) with the eventual goal of deriving highly accurate position of sufficiently radio-loud quasars from VLBI observations in the absolute astrometry mode. The original observing sample consisted of 447 optically bright, relatively weak extragalactic radio sources with declinations above -10° . The detailed observing scheme of this project is presented in Bourda et al. (2008). The first VLBI observing campaign in 2007 resulted in detection of 398 targets with the European VLBI Network (EVN) (Bourda et al. 2010), although no attempt to derive their positions or produce images was made. During the second observing campaign a subset of 105 sources detected in the previous campaign was observed with the global VLBI network that comprises the VLBA and EVN observing stations with the goal of revealing their morphology on milliarcsecond scales from VLBI images (Bourda et al. 2011) for consecutive screening the objects with structure that potentially may cause non-negligible systematic position errors. Their positions were derived by Petrov (2011) and formed the OBRs-1 catalogue.

In 2010–2011 remaining 290 sources have been observed in the third campaign, hereafter called OBRs-2, with the global network that comprises the VLBA and EVN observing stations in a mode similar to the second campaign. I present here

Leonid.Petrov@lpetrov.net

¹ see <http://astrogeo.org/rfc>.

Table 1
Summary of observing sessions

2010.03.23	gc034a	48	97
2011.11.08	gc034bcd	58	118
2011.03.15	gc034ef	40	77

Note. — The columns are: 1) epoch of an observing session, 2) session ID, 3) total session duration in hours excluding maintenance gaps, and 4) the number of program sources.

results of data analysis of this observations. Observations and their analysis are described in sections 2 and 3. The position catalogue is presented in section 4 and discussed in section 5. Concluding remarks are given in section 6.

2. OBSERVATIONS

During OBRS–2 campaign there were three observing sessions with 10 VLBA stations and 5–6 EVN stations from this list: EFLSBERG, MEDICINA, ONSALA60, YEBES40M, DSS63, HARTRAO, NOTO. First four EVN stations participated in every experiment, three remaining stations participated in some experiments. Each program source was observed in one session, in 3–4 scans, each 5 minutes long. Two sources, 1148+387 and 1203+109, were observed in two sessions in 5 scans. In addition to 290 program sources, 8 strong calibrators were observed.

Observations were made at X and S bands simultaneously. Data were sampled with 2 bits per sample at the aggregate rate of 512 Mbit/s. The intermediate frequencies were selected to provide continuous bandwidth [8.37699, 8.44099] and [2.22699, 2.29099] GHz. Such a setup is not favorable for astrometry. Spanning frequencies over 500 MHz, as it done in all other dual-band absolute astrometry VLBA surveys, improves precision of group delay determination, and therefore, source position precision *by one order of magnitude*. The position accuracy of sources observed with a wide-band frequency setup and detected at baselines 3,000–8,000 km long is limited by systematic errors. The position accuracy of sources observed in a frequency band spanned over 64 MHz is limited by the thermal noise.

Second limitation of the OBRS–2 schedule for the astrometry use is a relatively rare observation of sources at low and high elevations for better estimation of the troposphere path delay in zenith direction, which increases systematic errors. VCS1 survey (Beasley et al. 2002) suffered a similar deficiency in design, and analysis revealed systematic errors at a level of 0.4–0.5 mas. We can assume systematic errors of OBRS–2 were at a similar level. But since the contribution of the thermal noise in the error budget of OBRS–2 experiments is one order of magnitude higher than in VCS experiments, these increased systematic errors did not cause a noticeable further accuracy degradation.

Of 290 program objects, 58 sources were observed and detected in other absolute astrometry programs, such as Very Long Baseline Array (VLBA) Calibrator Survey (Beasley et al. 2002; Fomalont et al. 2003; Petrov et al. 2005, 2006; Kovalev et al. 2007; Petrov et al. 2007), regular VLBA geodetic observations (Petrov et al. 2009; Pushkarev & Kovalev 2012), and ongoing VLBI observations of 2MASS galaxies (Condon et al. 2011). Positions of all but four sources 0106+315, 0809+483, 1213+097, and 2247+140, are known with accuracy better than 0.4 mas. These 54 program sources and 8 calibrators provided a sufficient overlap

for tying position estimates to the existing catalogue and for evaluation of position accuracy.

3. DATA ANALYSIS

The data were correlated with DiFX software correlator (Deller et al. 2011) at the National Radio Astronomy observatory. The correlator computed the spectrum of cross correlation and autocorrelation functions with a frequency resolution of 0.25 MHz at accumulation intervals of 1 s long.

3.1. Preliminary analysis

The procedure of further analysis is described in full detail in Petrov et al. (2011a). I present here only a brief outline. First, log files are parsed, system temperature and phase calibration are analyzed, and points with outliers are removed. No phase calibration signal for non-VLBA stations was recovered due to a limitation of the DiFX correlator (which was lifted later in 2011). Next, the fringe amplitudes were corrected for a distortion in the sampler due to digitization. Then, the amplitudes were calibrated by multiplying them by the a priori

System Equivalent Flux Density (SEFD) $\sqrt{\frac{g_1 g_2}{T_{\text{sys}1} T_{\text{sys}2}}}$, where

g_i and $T_{\text{sys}i}$ are the gain and system temperature of the i th antenna respectively. Then a group delay, phase delay rate, group delay rate, and fringe phase were determined for every observations for each baseline at X and S bands separately using the wide-band fringe fitting procedure. These estimates maximize the amplitude of the cross-correlation spectrum coherently averaged over all accumulation periods of a scan and over all frequency channels in all intermediate frequency of a band. After the first run of fringe fitting, 12 observations at each baseline with a reference station with the strongest signal to noise ratios (SNRs) were used to adjust the station-based complex bandpass corrections, and the fringe fitting procedure with the bandpasses applied was repeated. This part of analysis is done with *PLMA* software².

Further analysis was split into two routes: astrometric and imaging. Following the astrometric route, total group delays and phase delay rates were computed on a common fringe reference time epoch within a scan using results of fringe fitting. These observables, along with auxiliary information describing observations, were exported to the VTD/post-Solve VLBI analysis software³ for interactive analysis. Initially, only observables with the high SNR to ensure that the probability of false detection is less than 0.001 were chosen. This SNR threshold is 5.8 for OBRS–2 experiments. Detailed description of the method for evaluation of the probability of false detection can be found in (Petrov et al. 2011a).

Then, theoretical path delays were computed according to the state-of-the art model as well as their partial derivatives. Small differences between group delays and theoretical path delay were used for estimation of corrections to a parametric model that describes the perturbation of the theoretical model using least squares (LSQ). Coordinates of target sources, positions of all stations, except the reference one, parameters of the spline with the time span of 1 hour that models corrections to the a priori path delay in the neutral atmosphere in the zenith direction for all stations, and parameters of another spline with the same time span that describes the clock function for all stations but the reference one were solved for

² Available at <http://astrogeo.org/pima>.

³ Available at <http://astrogeo.org/vtd>.

in separate least square solutions that used group delays at X and S bands respectively.

The dataset was cleaned for outliers, i.e. observations with residual group delays exceeding 5σ . The most common reasons for an observation to have a large residual are a failure of fringe fitting procedure to find the main maximum, the presence of radio interference, or false detection. Simultaneous solving for source positions with only few detections in a presence of outliers poses a certain risk. One bad observation may corrupt the solution, and as a result, remaining good observations of that source may get high residuals and the outlier elimination procedure may discard them. Identifying that bad observation(s) often required several trials. When the dataset was cleaned, I gradually lowered the SNR limit from 5.8 to 5.0 with a step of 0.1. The status of all observations with $\text{SNR} < 5.8$ was initially set to “suppressed”. That means these observations did not contribute to estimation of the parametric model, but the parametric model evaluated at the previous step was applied for computing their residuals. Suppressed observations with residuals by modulo less than 5σ at S band and less than 4σ at X band were restored one by one starting with the smallest normalized residual. After flipping the status “suppressed”, the LSQ solution was updated for including this observation into the parameter estimation model, and the process was repeated. There was a significant fraction of false detections with $\text{SNR} < 5.8$. But such observations have random group delay estimates uniformly distributed over $4\mu\text{s}$ wide search window. The probability that the group delay from a false detection will have a residual within 2–5 ns of the expected value, and therefore may be identified as a good observation, is an order of $1-2 \cdot 10^{-3}$. Suppression of observations with huge residual delay rates (several such points were found) allows to reduce this probability even further.

Then the fringe fitting procedure was repeated with a narrow fringe search window for those points that were marked as outliers. The center of fringe search window over delay and delay rate was set to the expected value of the delay and delay rate computed as a sum of the a priori delay or delay rate and the contribution from the parametric model derived during the LSQ adjustment. The width of the search window was set to 5 ns for S band and 3 ns for X band. In addition to that, I re-ran the fringe fitting procedure with the updated a priori model for all the sources that have position adjustments exceeding $1''$. For instance, 0744+092 had the a priori position $4.''8$ off the VLBI position. When a source has a large position error, a non-linear fringe phase change over a scan of 300 s long becomes significant and causes noticeable de-correlation.

The interactive analysis procedure was repeated with updated results of fringe fitting. The SNR threshold was lowered to 4.8 because the probability of false detection is less for a narrow fringe search window. The procedure of outliers elimination was repeated. Baseline dependent additive weight corrections were computed in such a way as the ratio of the weighted sum of post-fit residuals to their mathematical expectation was close to unity. This computation procedure is described in full detail by Petrov et al. (2009).

3.2. Multiple sources

Careful analysis revealed five sources that had more than 15% points with $\text{SNR} > 5.8$ marked as outliers that were not diagnosed as radio interference or errors in fringe fitting. These sources had different positions derived from X and S-band group delays. If to invert suppression status of points for

these sources, i.e. to restore a point that was suppressed and suppress the point that was used in the solution, and to re-run the procedure of outlier elimination then we can get a position that is consistent to a position at the opposite band. These can be explained if to suggest that a sources has multiple components separated at an arcsecond level, strong enough to be detected. I used the following technique for component separation in order to investigate these sources. I cloned visibilities of these sources and treated them as different objects with different positions. Using their preliminary positions as a priori, a shifted phases of visibilities to the new positions and performed the fringe search in a narrow window, the same way as I treated outliers. This approach yielded a significant number of new detections for both components at one or both bands. New detections confirmed the hypothesis that a source is multiple.

3.3. Global astrometric solution

The result of the interactive solution provided a clean dataset of X and S-band group delays with updated weights. The dataset that was used for the final parameter estimation utilized all dual-band S/X data acquired under the absolute astrometry and space geodesy programs from April 1980 through December 2012, including 76079 observations from OBRS-2 experiments, in total 8.89 million observations. As I mentioned, among program sources, 58 common objects were observed in other absolute astrometry VLBI experiments. I made four solutions. The first three solutions used the global dataset, except observations of 58 common objects, and observable from the OBRS-2 experiments: 1) the first solution used the X-band group delays, 2) the second solution used the S-band group delays, and 3) the third solution used the ionosphere free linear combinations of X and S-band group delays. The fourth reference solution used all experiments in the global dataset with the only exception of OBRS-2 data.

OBRS-2 experiments were analyzed exactly the same way as 5497 other VLBI observing sessions, using the same analysis strategy that was used for processing prior observations for ICRF (Ma et al. 1998), VCS, VGaPS, Long Baseline Array Calibrator Survey (LCS) (Petrov et al. 2011b), and K/Q survey (Lanyi et al. 2010) catalogues. The estimated parameters are right ascensions and declination of all sources, coordinates and velocities of all stations, coefficients of B-spline expansion of non-linear motion for 26 stations, coefficients of harmonic site position variations of 48 stations at 4 frequencies: annual, semi-annual, diurnal, semi-diurnal, and axis offsets for 69 stations. Estimated variables also included Earth orientation parameters for each observing session, parameters of clock function and residual atmosphere path delays in the zenith direction modeled with the linear B-spline with interval 60 and 20 minutes respectively. All parameters were adjusted in a single LSQ run.

The system of LSQ equations has an incomplete rank and defines a family of solutions. In order to pick a specific element from this family, I applied the no-net rotation constraints on the positions of 212 sources marked as “defining” in the ICRF catalogue that required the positions of these sources in the new catalogue to have no rotation with respect to their positions in the ICRF catalogue. No-net rotation and no-net-translation constraints on site positions and linear velocities were also applied. The specific choice of identifying constraints was made to preserve the continuity of the new catalogue with other VLBI solutions made during last 15 years.

3.4. Image analysis

The same dataset of visibilities was used for source imaging. At first, I discarded all visibilities from observations that were marked as outliers in the final step of the interactive analysis procedure. Next, the data should be averaged over time and frequency after phase rotation for the contribution of group delay, group delay rate, and phase delay rate found by the fringe search procedure. Since the fringe fitting procedure was baseline-based, the baseline-dependent parameters of fringe fitting should be transformed to station-based parameters in order to preserve phase closures of visibilities. This transformation was done for the visibilities of each scan, each subarray, and each band separately. Although the experiments were scheduled for all the stations of the network to observe the same source during scan time, it may happen that some sources were detected only at a subset of baselines that do not have common stations. For each scan I found a scan-reference time as a weighted mean epoch of used observations. I selected a reference station for each subarray and solved with least squares for station-dependent group delays, group delay rates, and phase delays using baseline-dependent estimates of these quantities found by the fringe search procedure as the right-hand-side. These station-dependent quantities related to a common epoch within a scan were used for phase rotating the visibilities. After phase rotation, the visibilities were averaged over 32 spectral channels in each intermediate frequency and over 4 s intervals.

The averaged visibilities and accompanying weights were split into sources and written in separate files. Further processing was done using DIFMAP software package (Shepherd 1997). I used automatic imaging procedure *mupet* developed by Martin Shepherd and Greg Taylor. It started from a point source model as an initial guess and performed a sequence of image cleaning, phase and amplitude self-calibrations with and without taper.

I developed a web application that allowed me to inspect images visually and flag those that showed visible artifacts. Of 564 images made automatically, I selected 63 images that I processed interactively. These were the sources that either had points with amplitude outliers that an automatic procedure was unable to flag out or sources with too few observations, in a range of 15–35, when an automatic procedure of hybrid imaging becomes unstable. In total, images were produced for 279 sources at X band and for 285 sources at S band⁴. As a measure of a source strength, I derived two quantities from source brightness distributions: I computed the median correlated flux densities at baselines with projection lengths shorter than 900 km and the median correlated flux densities for baselines with projection lengths longer than 5000 km.

Some weak sources have too few points for successful imaging. In order to provide a measure of source strength at long and short baselines for these objects, I made a simplified amplitude analysis similar to what was done in processing OBRS–1 observations. I used averaged corrections to gains evaluated during self-calibration of strong sources and applied these corrections to the a priori SEFDs. From fringe amplitudes calibrated this way I computed the median correlated flux densities at baselines with projection lengths shorter than 900 km and for baselines with projection lengths

longer than 5000 km, similar to what I did in image processing. Comparison of estimates of median correlated flux densities of strong sources derived by this method with estimates of correlated flux densities derived from images produced by a rigorous self-calibration procedure showed they agree at a level of 15%.

Detailed analysis of produced images goes beyond the scope of the present paper and will be given in the future in a separate publication (G. Bourda et al., 2013, paper in preparation).

4. RESULTS

I have detected at least at one band all but one source 0843–025 (J0845–0241). In present paper objects with multiple components are treated as different sources, although most likely these are parts of the same objects.

Since 58 of 295 detected sources have been observed with VLBA in different programs at X band in a wide-band mode with frequency spanned over 494 and 992 MHz, their position uncertainties are a factor of 10–20 better than the position uncertainties from OBRS–2 experiments with the same SNR and the same number of observables. Therefore, for the purpose of comparison with OBRS–2 catalogue, positions of these sources can be considered as precisely known. I excluded from comparison 4 sources that are resolved and had uncertainties exceeding 0.4 mas in the reference solution.

Comparison showed that the solution that used ionosphere free linear combinations of X/S group delay observables did not improve the agreement between position estimates of 54 common sources with respect to the solution that used X-band only observables. The position uncertainties of OBRS–2 observations are too large for the residual ionosphere contributions to affect positions at a significant level. I computed the variance that, being added in quadrature to source position uncertainties, makes the ratio of the sum of weighted squares of position differences to their mathematical expectations close to unity. These variances are 1.7 mas in right ascension and 2.1 mas in declination for the X-band solution, and 2.1 mas in right ascension and 2.4 mas in declination for the S-band solution.

4.1. OBRS–2 catalogue

The majority of sources were detected at both bands, and there are position estimates from two solutions that used X-band and S-band observables from the OBRS–2 experiments. The preference was given to the solution that used X-band observables because first, the detection limit at X band was lower and second, the contribution of the residual ionosphere after applying reduction for the total electron contents from GPS observations at X band is one order of magnitude less than at S band. If the reweighted position uncertainty from the S-band solution was at least a factor of 1.5 smaller than the uncertainty from the X-band solution, the position from the S-band solution was used in the final catalogue. Although there are additional more precise observations of 58 common sources in other absolute astrometry experiments, these observations were excluded in solutions 1 and 2 used for deriving the OBRS–2 catalogue.

The positions of 295 sources observed in OBRS–2 experiment are listed in Table 2. The 1st and 2nd columns provide the IVS source name (B1950 notation) and IAU name (J2000 notation). The 3rd and 4th columns give source coordinates at the equinox on the J2000 epoch. Columns 5 and 6

⁴ Images in FITS format as well as calibrated visibilities are available at <http://astrogeo.org/obrs>.

Table 2
First 8 rows of the OBRS–2 source position catalogue.

IAU name		Source coordinates			Position errors			# pnt		F_{corr} S band		F_{corr} X band		Flags		
B1950	J2000	α	δ		σ_α	σ_δ	corr	band	S	X	short	unres	short	unres	S	X
		hr mn sec	°	'	''	mas	mas				Jy	Jy	Jy	Jy		
J0001+0632	2358+062	00 01 23.694601	+06 32 30.93754			3.52	15.24	−0.811	X	38 31	0.018	0.022	0.018	0.008	m	m
J0005+1609	0003+158	00 05 59.237650	+16 09 49.02157			1.86	2.53	−0.342	X	168 168	0.143	0.070	0.196	0.057	m	m
J0015+3052	0012+305	00 15 36.022281	+30 52 29.79522			2.98	7.35	−0.437	X	12 32	0.026	0.015	0.017	0.006		
J0017+1451	0015+145	00 17 36.903866	+14 51 01.88067			1.92	3.10	−0.557	X	164 166	0.065	0.039	0.053	0.030	m	m
J0027+4514	0025+449	00 27 42.262713	+45 14 57.07879			2.72	2.88	−0.477	X	222 129	0.048	0.042	0.024	0.015	m	m
J0035+1553	0033+156	00 35 55.537977	+15 53 16.45642			23.81	23.11	−0.267	S	29 3	0.074	<0.017	−1.00	−1.00		
J0037+3938	0034+393	00 37 36.725767	+39 38 11.79014			2.44	2.86	−0.354	X	210 121	0.142	0.044	0.039	0.012	m	m
J0041−0143	0038−019	00 41 26.008767	−01 43 15.67847			2.03	5.16	−0.625	X	143 125	0.056	0.049	0.037	0.032	m	m

Note. — Units of right ascension are hours, minutes and seconds. Units of declination are degrees, minutes and seconds. (This table is available in its entirety in machine-readable and Virtual Observatory (VO) forms in the online journal. A portion is shown here for guidance regarding its form and content.)

give reweighted source position uncertainties in right ascension and declination in mas (without $\cos\delta$ factor), and column 7 gives the correlation coefficient between the errors in right ascension and declination. Column 8 shows band ID of the solution that was used to derive position of a given source. The number of group delays used in analysis is listed in columns 9 and 10. Columns 11 and 12 provide the median value of the correlated flux density in Jansky at S band at baseline projection lengths shorter than 900 km and at baseline projection lengths longer than 5000 km. The latter estimate serves as a measure of the correlated flux density of an unresolved source component. Columns 13 and 14 provide the median of the correlated flux density at X band at baselines shorter than 900 km and longer than 5000 km. If no information about correlated flux density is available, -1.000 is used as a placeholder. The last two columns have flags whether an image is available for S and X bands: “m” if available, blank if not.

The semi-major axes of error ellipses range from 2.1 to 200 mas, with the median 3.2 mas, and for 80% sources the position errors are under 5.2 mas. The major factor that results in position uncertainty exceeding 5 mas is a lack of detections at long baselines. Sources with large position uncertainties are either highly resolved or very weak moderately resolved objects.

4.2. Analysis of multiple sources

0154+31A/0154+31B has two components $2''.592$ apart. Component A is compact and was detected at 5 mJy level at X band at intercontinental baselines with Effelsberg. It was not detected at intercontinental baselines at S band. Since the sensitivity of baselines with Effelsberg is a factor of 4–5 worse at S band than at X band, this can be explained if a source has a spectral index steeper than -1.1 ($S \sim f^\alpha$). Component B is stronger at S band, but has only three detections at 5 mJy level at X band at short baselines only. Cross-matching against Wide-field Infrared Survey Explorer (WISE) infrared catalogue of point sources (Wright et al. 2010) revealed WISE J015715.32+315419.2 object with magnitude 13.9 at 3.6μ within $0''.36$ of 0154+31A.

0809+483/0809+48B/0809+48C has three components within $6''$. Components B and C coincide with extended radio-lobes visible at the VLA image (Figure 1). Compact component A that has X-band flux density 5 mJy at intercontinental baselines is located between radio lobes. WISE J081336.05+481302.7 with magnitude 13.5 at 3.6μ was found within $0''.11$ of component A.

1323+65A/1323+65B has two components with separa-

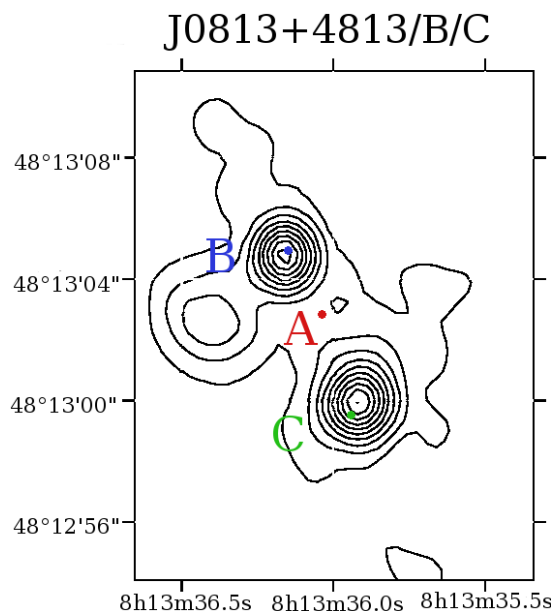


Figure 1. Triple source 0809+483/0809+48B/0809+48C VLA image at 4.86 GHz on epoch 1995.10.15 with beam size $1''.27$, project AS561, is shown as a contour map. VLBI positions are shown with filled circles. Component A is the most compact and has flux density 5 mJy at intercontinental baselines. Components B and C are resolved and visible only at short baselines.

tion $3''.157$. Although component B is 5 times stronger at X band at the VLA image (Figure 2) than component A — 21 mJy versus 4 mJy, it is not detected at VLBA scale at X band. Component A with correlated flux density 4 mJy at intercontinental baselines lies within $0''.20$ of WISE J132529.70+651513.3 which has magnitude 14.6 at 3.6μ .

1335−06A/1335−06B has two components $4''.896$ apart. Component B, associated with a radiolobe (Figure 3) was detected at S band only. Compact component A with flux density 7 mJy at X band is within $0''.18$ of WISE J133807.98−062711.0, which has magnitude 13.9 at 3.6μ .

1340+60A/1340+60B has two components separated at $3''.014$. The source looks elongated at the VLA image at 1.4 GHz (Figure 4). Component B was detected at S band only. Component A is within $0''.23$ of WISE J134213.26+602142.9 which has magnitude 14.2 at 3.6μ .

5. DISCUSSION

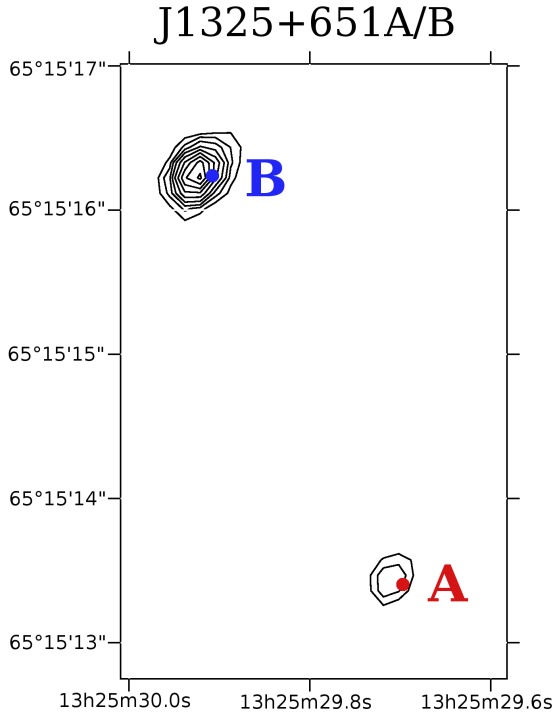


Figure 2. Double source 1323+65A/1323+65B VLA image at 8.4 GHz on epoch 1999.08.08 with beam FWHM $0.''27$, project AR415, is shown as a contour map. Although component B is stronger at the VLA image, it is resolved out at X band at VLBA resolution. Component A has flux density 27 mJy at both bands.

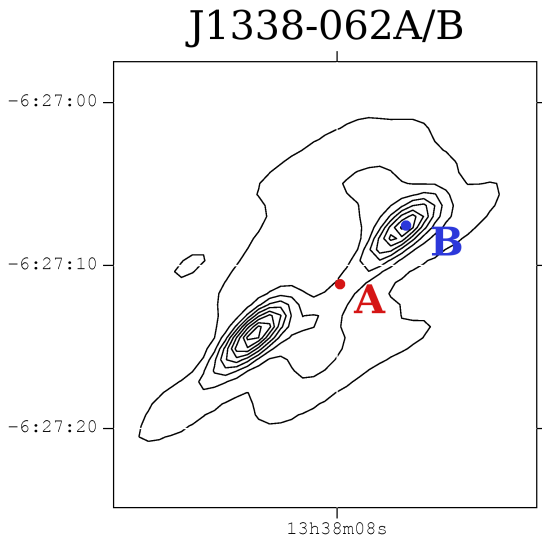


Figure 3. Double source 1323+65A/1323+65B at the VLA image at 1.4 GHz on epoch 2001.04.29 with beam size $6.''45$, project AB950 (FIRST), is shown as a contour map. Component B was detected in OBRs-2 only at S band.

Position accuracy, 2–5 mas for 80% OBRs-2 sources, is too coarse to make a meaningful comparison with *Gaia* because the frequency setup was not favorable for precise absolute astrometry.

Cross-referencing the cumulative catalogue of radio sources detected with VLBI in the absolute astrometry mode at 8 GHz against the optical catalogue of active galaxy nuclei, including quasars, of Veron-Cetty & Veron (2010), I

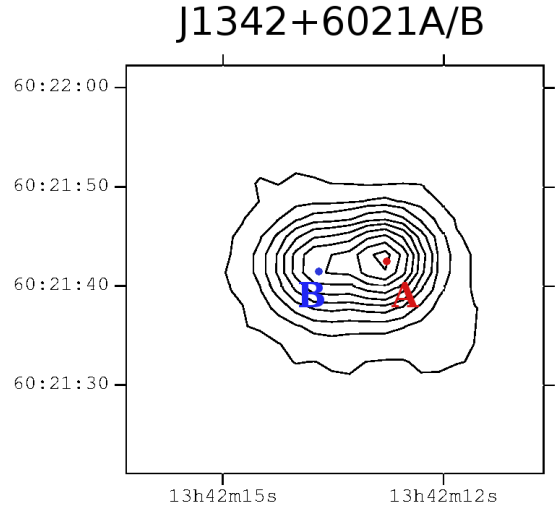


Figure 4. Double source 1340+60A/1340+60B VLA image at 1.4 GHz on epoch 2002.02.07 with beam size $5.''4$, project AB950 (FIRST), is shown as a contour map. Component B was detected only at S band.

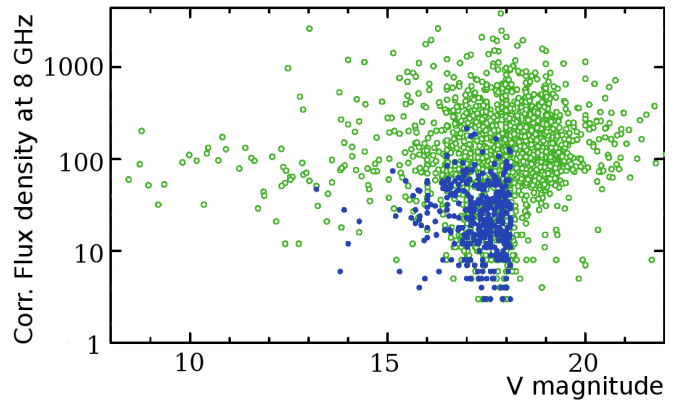


Figure 5. Dependence of the median correlated flux density at 8 GHz at baselines longer than 5000 km versus V magnitude of those active galaxy nuclei that have been detected with VLBI under absolute astrometry programs. Solid blue filled circles show sources detected at X band at OBRs-1 and OBRs-2 campaigns. Green hollow circles show associated sources observed under other programs.

found that 1676 objects, or 23%, have a counterpart within a $4''$ search radius. Of them, 825 objects are brighter V 18^m mag. Of them, 377, or 46%, were observed in OBRs-1 or OBRs-2 programs, and 293 of them were observed only in these two programs. Five OBRs-2 sources, 0012+305, 0232-042, 0744+092, 1146+249, 1632+198 have position offsets with respect to the optical catalogue of quasars of Veron-Cetty & Veron (2010) exceeding $4''$. Since their offsets with respect to WISE catalogue are in a range of $0.08''$ – $0.43''$, I consider that their positions in the optical catalogue had an error.

Figure 5 shows the dependence of the correlated flux density versus V magnitude for the entire sample of radio-optical associations and for the sub-sample observed in the OBRs-1 and OBRs-2 programs. There is no sign of obvious correlation between optical brightness and radio brightness. We see that the OBRs-1/OBRs-2 sources are systematically weaker than those observed in other programs. Of 400 sources detected in OBRs-1 and OBRs-2, only 148 have an unresolved component at X band stronger than 30 mJy, while the to-

tal number of radio sources associated with quasars brighter V 18^m mag and with unresolved component stronger than 30 mJy is 683.

If a source is too weak at long baselines, the position uncertainty 0.1 mas will not be achieved for a reasonable integration time because of the thermal noise. The median semi-major axis of the position error ellipse of OBRS–1/OBRS–2 sources without reweighting is 2.2 mas. The frequency sequence used in these observing programs results in a group delay uncertainty at a given SNR that is a factor of 11.2 greater than the group delay uncertainty of regular geodetic observations under RDV program. Even if OBRS programs were observed with the same frequency sequence as RDV experiments, the median position uncertainty due to the thermal noise would have been 0.2 mas. Therefore, future observations for improving source positions associated with optically bright quasars should be focused on observing compact radio sources with a strong unresolved core. *The majority* of such objects were detected in program *other* than OBRS–1/OBRS–2. Therefore, program OBRS can be considered as partially successful. Observing sources known as weak from the EVN detection survey (Bourda et al. 2010) was not warranted for the goal of the project. Selection of a frequency sequence that is unfavorable for astrometry degraded position accuracy by one order of magnitude but did not bring any merit.

The VLBI catalogue is complete only to flux densities 180 mJy (Petrov et al. 2013). Figure 5 suggests there may exist other strong radio sources associated with optically bright quasars. Systematic surveys targeted to sources with correlated flux densities at long baselines in a range of 50–180 mJy promise to reveal new radio loud quasars. If to observe each target source for 2 minutes at 512 Mbit/s at X/S in two scans each at the VLBA, \sim 1800 sources with correlated flux densities down to 25 mJy could be observed for 242 hours allotted for OBRS–1, OBRS–2, and the EVN detection survey. This approach is an alternative to the strategy adopted for OBRS project.

6. SUMMARY

Analysis of the second dual-band S/X VLBA campaign of the program for observing optically bright extragalactic radio sources allowed me to determine positions of 295 target sources and make images of 285 of them. Because of using the frequency setup unfavorable for absolute astrometry, the position uncertainties ranged from 2 to 200 mas with the median value of 3.2 mas. Many these sources are suitable as phase calibrators.

This position accuracy is sufficient for using these sources as phase calibrators, but not sufficient for drawing meaning-

ful conclusions from comparison of *Gaia* and VLBI positions. Approximately 1/3 of observed sources have strong unresolved core and their positions can be determined with accuracies better than 0.1 mas in future VLBI observing programs with appropriate frequency setup.

The National Radio Astronomy Observatory is a facility of the National Science Foundation operated under cooperative agreement by Associated Universities, Inc. This publication makes use of data products from the Wide-field Infrared Survey Explorer, which is a joint project of the University of California, and the JPL/California Institute of Technology, funded by the NASA.

Facilities: VLBA (project code GC034).

REFERENCES

- Beasley, A. J., Gordon, D., Peck, A. B., et al. 2002, *ApJS*, 141, 13.
 Bourda, G., Charlot, P., & Le Campion, J.-F. 2008, *A&A*, 490, 403
 Bourda, G., Charlot, P., Porcas, R. W., Garrington, S. T., 2010, *A&A*, 520, 113
 Bourda, G., Collioud, A., Charlot, P., Porcas, R. W., Garrington, S. T. 2011, *A&A*, 526, A102
 Charlot, P., Fey, A. L., Collioud, A., et al. 2007, in Proceedings of the Journées Systèmes de Référence Spatio-temporels 2007. Observatoire de Paris, 17-19 September 2007, ed by N. Capitaine, p 8
http://synte.obspm.fr/jsr/journees2007/pdf/s1_02_Charlot.pdf
 Cohen M. H. & Shaffer D. B. 1971, *AJ*, 76, 91.
 Condon J., Darling J., Kovalev Y. Y., Petrov L. 2011, preprint <http://arxiv.org/abs/1110.6252>
 Deller, A., Brisken, W. F., Phillips, C. J., et al. 2011, *PASP*, 123, 275
 Fomalont, E., Petrov, L., McMillan, D. S., et al. 2003, *AJ*, 126, 2562.
 Kovalev, Y. Y., Petrov, L., Fomalont, E., Gordon, D. 2007, *AJ*, 133, 1236.
 Kovalev, Y. Y., Lobanov, A. P., Pushkarev, A. B., Zensus, J. A. 2008, *A&A*, 483, 759
 Lanyi, G. E., Boboltz, D. A., Charlot, P., et al. 2010, *AJ*, 139, 1695
 Lindegren, L., Babusiaux, C., Bailer-Jones, C., et al. 2008, in Proc. IAU Symposium, 248, 217
 Ma, C., Arias, E. F., Eubanks, T. M., et al. 1998, *AJ*, 116, 516
 Matveenko, L. I., Kardashev, N. S., Sholomitskii, G. B. 1965, *Izvestia VUZov. Radiofizika*, 8, 651 (English transl. *Soviet Radiophys.*, 8, 461)
 Petrov, L., Kovalev, Y. Y., Fomalont, E., Gordon, D. 2005, *AJ*, 129, 1163
 Petrov, L., Kovalev, Y. Y., Fomalont, E., Gordon, D. 2006, *AJ*, 131, 1872
 Petrov, L., Kovalev, Y. Y., Fomalont, E., Gordon, D. 2007, *AJ*, 136, 580
 Petrov, L., Gordon, D., Gipson, J., et al. 2009, *Jour. Geod.*, 83, 859
 Petrov, L. 2011, *AJ*, 142, 105
 Petrov, L., Kovalev, Y. Y., Fomalont, E., Gordon, D. 2011a, *AJ*, 142, 35
 Petrov, L., Phillips, C., Bertarini, A., Murphy, T., Sadler, E. M., 2011b, *MNRAS*, 414(3), 2528
 Petrov L., et al., 2013 submitted to *MNRAS*
 preprint <http://arxiv.org/abs/1301.2386>
 Porcas, R. W. 2009, *A&A*, 505, L1
 Pushkarev, A. B., Kovalev, Y. Y. 2012, *A&A*, 544, 34
 Shepherd, M. C. 1997, in ASP Conf. Series, 125, *Astronomical Data Analysis Software and Systems VI*, ed. by G. Hunt & H. E. Payne (San Francisco: ASP), 77.
 Sokolovsky, K. V., Kovalev, Y. Y., Pushkarev, A. B., & Lobanov, A. P. 2011, *A&A*, 532, A38
 Veron-Cetty, M. P., Veron, P. 2010, *A&A*, 518, A10
 Wright, E. L., Eisenhardt, P. R. M., Mainzer, A. K., et al. 2010, *AJ*, 140, 1868